Journal of Nuclear Materials 386–388 (2009) 231–235

Contents lists available at ScienceDirect

Journal of Nuclear Materials

journal homepage: www.elsevier.com/locate/jnucmat

Hardening mechanisms of reduced activation ferritic/martensitic steels irradiated at 300 °C

Hiroyasu Tanigawa [a,*], Ronald L. Klueh [b], Naoyuki Hashimoto [c], Mikhail A. Sokolov [b]

[a] Japan Atomic Energy Agency, 2-4 Shirakata Shirane, Tokai, Ibaraki 319-1195, Japan
[b] Oak Ridge National Laboratory, Oak Ridge, TN, USA
[c] Hokkaido University, Sapporo, Hokkaido, Japan

A B S T R A C T

It has been reported that reduced-activation ferritic/martensitic steels (RAFMs), such as F82H, ORNL9Cr–2WVTa, and JLF-1 showed a variety of changes in ductile–brittle transition temperature and yield stress after irradiation at 300 °C up to 5 dpa, and those differences could not be interpreted solely by the difference of dislocation microstructure induced by irradiation. In this paper, various microstructural analyses on low-temperature irradiated RAFMs were summarized with the emphasis on F82H, and a possible mechanism for the irradiation hardening was suggested. The possible contribution of dislocation channeling structure and back stress were indicated.

© 2009 Elsevier B.V. All rights reserved.

1. Introduction

In reduced-activation ferritic/martensitic (RAFM) steels, irradiation hardening and embrittlement are induced by low-temperature irradiation, i.e., below 350 °C, and this is an issue for designing a water-cooled solid-breeder (WCSB) blanket system for a fusion reactor (Fig. 1). To design the WCSB system with such property changes, the phenomena must be predictable based on data and mechanistic understanding. This is mandatory for DEMO, as 14 MeV neutron irradiation effects (He, H effects) must be estimated. To achieve this, mechanistic understanding of these property changes based on microstructure is essential.

In this study, the current understanding on microstructural evolution under low-temperature irradiation is reviewed mainly based on the database of F82H. For this discussion, irradiation data (300 °C/5 dpa) will be used that was obtained from specimens irradiated in the removable beryllium (RB) position of the High Flux Isotope Reactor at the Oak Ridge National Laboratory, USA [1]. With these data, in which irradiation temperature history was well defined, the essential microstructure features that dominate mechanical property changes were identified, and a possible mechanism of hardening was proposed.

2. Microstructure changes

2.1. Normalized-and-tempered microstructures

RAFM steels are fully tempered martensitic steels, in which the microstructures contain prior-austenitic grain (PAG) boundaries, martensite packet, block, and lath boundaries which formed during normalization, and precipitates, mainly $M_{23}C_6$, which formed during tempering. This microstructure gives the steel high irradiation and heat resistance (Fig. 2). F82H is a RAFM steel with a nominal chemical content of Fe–8Cr–2W–0.2V–0.04Ta; it is normalized by austenitizing at 1040 °C for 40 min followed by an air cool, and it is tempered at 750 °C for 1 h.

Dislocation density will vary depending on the heat treatment condition, and the typical dislocation density after the aforementioned heat treatment is about $2–3 \times 10^{21}$ ($1/m^2$). Precipitates are a major microstructural feature in RAFM steels besides dislocations, as shown in Fig. 3. These precipitates on boundaries block dislocation glide by acting as two-dimensional obstacles to dislocation motion. This is confirmed by the microstructure of the tip of a fractured tensile specimen (Fig. 4), as it still shows the martensite lath structure even at the very last stage of plastic deformation.

2.2. Irradiated microstructures

It has been reported that the major microstructural feature of RAFMs irradiated at low temperatures is dislocation loop formation and evolution [2–4]. Fig. 5 shows the dislocation microstructure evolution observed in the high-voltage electron microscope (HVEM) operated at 1250 kV at 300 and 400 °C. The observations

* Corresponding author. Tel.: +81 29 282 6498; fax: +81 29 284 3589.
E-mail address: tanigawa.hiroyasu@jaea.go.jp (H. Tanigawa).

0022-3115/$ - see front matter © 2009 Elsevier B.V. All rights reserved.
doi:10.1016/j.jnucmat.2008.12.094

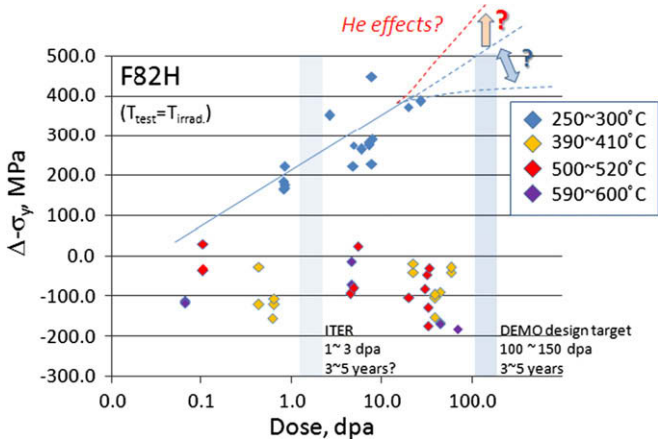

Fig. 1. Dose dependence of irradiation hardening at various irradiation temperatures. Test temperature is equal to irradiation temperature.

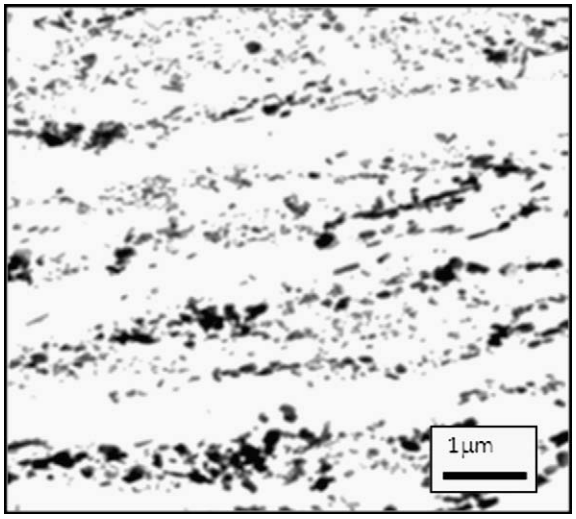

Fig. 3. TEM bright field image of F82H replica sample.

suggest that dislocation loop nucleation is dominant at 300 °C, and nucleation seems to be saturated over 1 dpa. Loop growth and dislocation climb appears to be the dominant microstructural evolution at 400 °C. This suggests that temperature control is essential, especially between 300 and 400 °C, and it confirms that dislocation loops are the major dislocation feature related to irradiation hardening.

TEM observations of neutron-irradiated RAFMs show that the dislocation loops with black dot contrast are the major dislocation microstructural feature at 300 °C after 5 dpa. Even though no aging effects were expected at 300 °C, extraction residue and replica analyses suggested possible changes on the distribution of precipitates [5,6], and chemical composition changes of these residues after irradiation were also reported [7]. In addition to this, the amorphization of precipitates or the nucleation of nano-sized precipitates (or both) had been reported on fission-, spallation- and ion-irradiated F82H [8–10]. On the other hand, no irradiation-induced segregation was observed in irradiated F82H (Fig. 6).

The deformed microstructure of irradiation-hardened F82H was examined [10], and the presence of dislocation channeling was reported (Fig. 7). Number density and average diameter of dislocation loops and precipitates are summarized in Table 1.

3. Discussion

3.1. Strength of normalized-and-tempered RAFMs

Since a lath boundary is a small-angle tilt boundary, precipitates on a lath boundary can be treated the same as precipitates in the matrix, i.e., an Orowan-type obstacle that exerts a friction stress against dislocation movement. On the other hand, precipitates on block, packet and PAG boundaries impede further dislocation glide and exert a back stress. This interpretation is supported by the TEM observations on the microstructure of the tip of fractured tensile specimen (Fig. 4), as boundaries are still observed in a deformed and fractured specimen. Also, the tensile specimen used to obtain irradiation data shown in Table 1 is a sheet specimen (SS-3) with aspect ratio of cross section (width/thickness) of 2, so it could be assumed that shear strain deformation is dominant during plastic flow. Thus, F82H is a precipitate-strengthened steel, and its flow stress, τ_{flow}, could be described as follows:

$$\tau_{flow} = \tau_i + \tau_b, \tag{1}$$

where τ_i is friction stress, and τ_b is back stress, and these will be described as [11,12]

$$\tau_i = \tau_p + k\sqrt{C} + \alpha G b\sqrt{\rho} + \alpha' G b\sqrt{N \cdot d}, \tag{2}$$

$$\tau_b = \frac{k_y}{\sqrt{D}}. \tag{3}$$

In Eq. (2), τ_p is the Peierls force, k is the hardening constant of solute with concentration C, α is a constant, and $\alpha = 0.3$ for dislocations, G is the shear modulus (80 GPa), b is the Burgers vector (0.268 nm), ρ is dislocation density, α' is a constant for precipitates with $\alpha' = 0.3$ in the matrix and lath boundaries with number density N and average diameter d. Eq. (3) is the Hall–Petch equation with D being the aver-

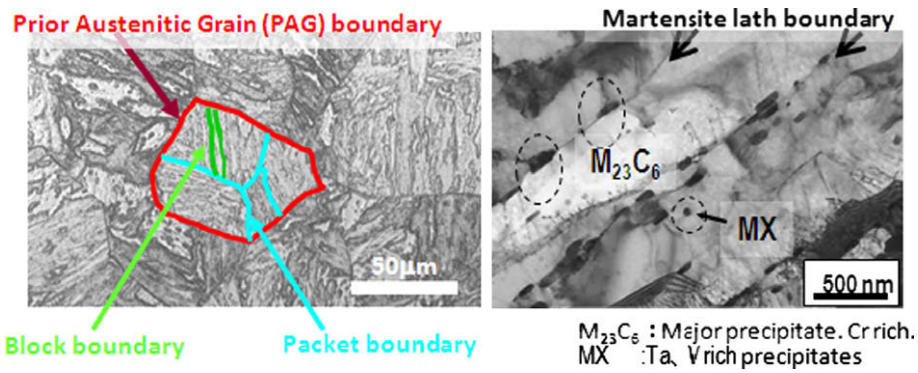

Fig. 2. Microstructure of normalized-and-tempered F82H, which is typical of all RAFM steels.

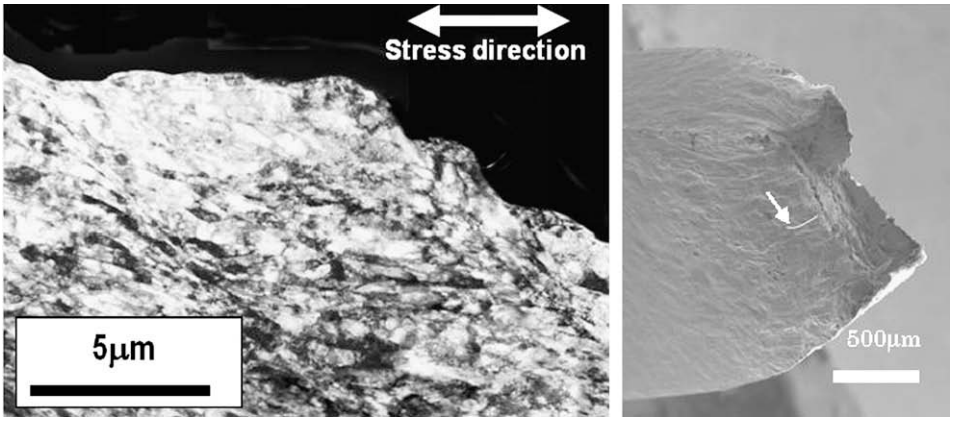

Fig. 4. TEM bright field image of fracture end of F82H tensile specimen. Sampled position was indicated in SEM images with white line.

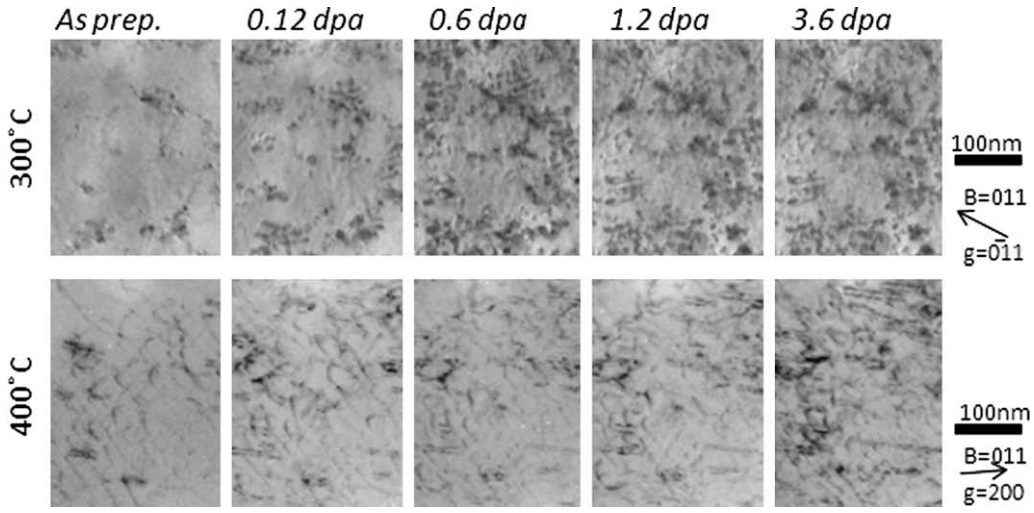

Fig. 5. TEM bright field images of HVEM-irradiated F82H at 300 and 400 °C .

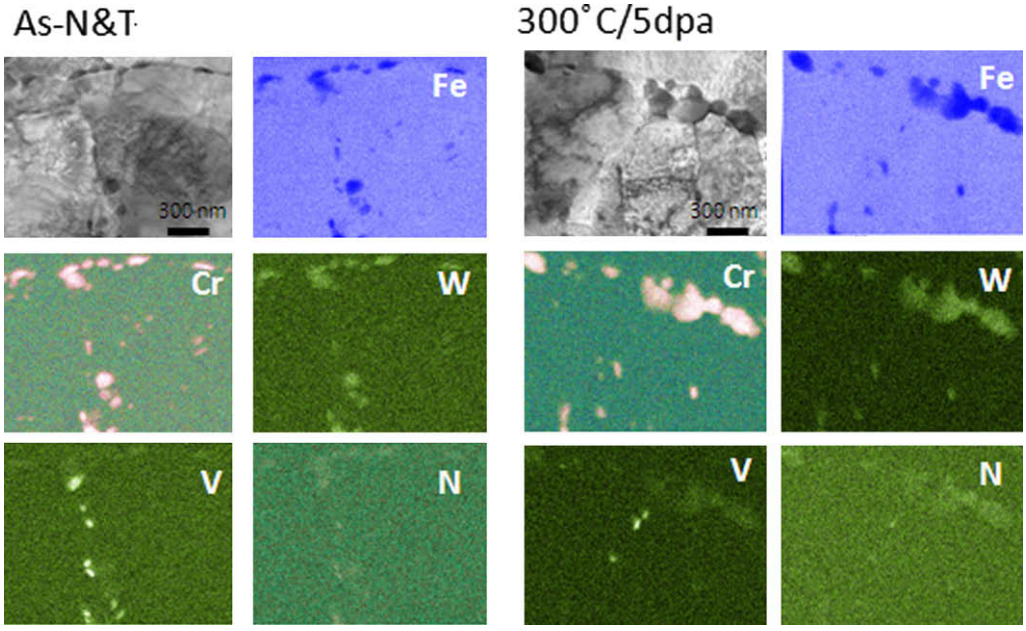

Fig. 6. Elemental mapping on normalized-and-tempered and irradiated F82H.

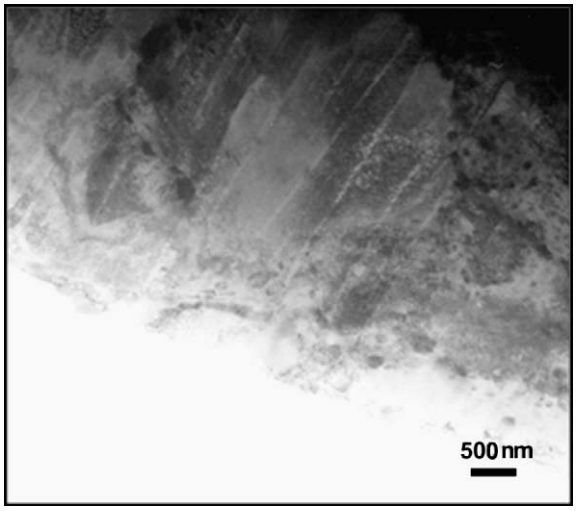

Fig. 7. TEM bright field images of F82H deformed after irradiation [16].

age distance of blocking boundary and k_y the dislocation-locking parameter described by,

$$k_y = \alpha'' \sqrt{Gb\tau_c}, \tag{4}$$

where α'' is a constant and τ_c is the critical shear stress which activates dislocation sources in the adjacent grain.If we assume yield occurs under von Mises conditions for a plate-type specimen under pure shear strain deformation and the defined yield condition is given as the stress level when the dislocation source in the adjacent grain is activated, then yield occurs when

$$\tau_{\text{applied}} \geq \tau_i + \tau_b, \quad \tau_{\text{applied}} = \tau_{\text{yield}} = \frac{1}{\sqrt{3}}\sigma_y, \tag{5}$$

where σ_y is the 0.2% proof stress. The yield process normally occurs at less than flow stress level and is controlled with the most dominant factor [12]. In a normalized-and-tempered (NT) RAFM, dislocations, which are introduced by the martensite transformation, and precipitates ($M_{23}C_6$), which are introduced during tempering, are the most dominant microstructural features. Since most of the precipitates were observed on boundaries, as shown in Figs. 2 and 3, it could be assumed that the precipitates work as two-dimensional obstacles to dislocation motion, rather than to assume them to be zero dimensional obstacles (Orowan obstacles).

For the case of F82H, yield stress, $\sigma_{y,}$ at room temperature is 528 MPa, and calculated τ_i based on dislocation density is 288–352 MPa, which is in good agreement with the measured yield stress level. This suggests that yield stress of a NT RAFM is determined by dislocation density, i.e.,

$$\tau_{\text{yield}} = 1/\sqrt{3}\sigma_y = \tau_i = \alpha Gb\sqrt{\rho} \tag{6}$$

and this is quite reasonable as it was indicated that the contribution of back stress to the yield process becomes negligible if there are enough obstacles against dislocation movements in a grain [13].

On the other hand, the work hardening process can be interpreted as the result of the back stress increase induced by dislocation pile-ups at boundaries during the work hardening. In this case, it could be assumed that, (a) flow stress is equal to ultimate stress (σ_u), $\tau_{\text{flow}} = \frac{1}{\sqrt{3}}\sigma_u$, and (b) critical shear stress is equal to ultimate stress, $\tau_c = \tau_{\text{flow}}$, and (c) the blocking boundary is a lath boundary, D = 300 nm, and then α'' in Eq. (4) is calculated to be 0.27–0.55 (Table 2).

3.2. Strength of low- temperature irradiated RAFMs

As shown in the previous section, dislocation loops are the major microstructural feature after low-temperature irradiation. The number density of dislocation loops is on the order of 10^{23}, and this leads to the conclusion that irradiation hardening is caused by dislocation loops, and this factor based on the Orowan equation is described as follows:

$$\Delta\tau_i(\text{loop}) = \alpha_{\text{loop}} Gb\sqrt{N_{\text{loop}} \cdot d_{\text{loop}}}, \tag{7}$$

where α_{loop} is constant and α_{loop} = 0.3 is the reasonable value derived from the hardening level observed in Fe–9Cr in which dislocation loops are the only major microstructural feature [14]. Hardening caused by dislocation loops was calculated (Table 2) based on the value presented in Table 1. It should be noted that possible dislocation loop type dependence of α_{loop}, i.e., $(a/2)\langle 1\,1\,1\rangle$

Table 1
Microstructrual features of normalized-and-tempered and irradiated (up to 5 dpa at 300 °C).

RAFM		F82H-IEA				ORNL9Cr				JLF-1			
Metallography	Prior austenite grain size (mm)	~100				~30				~50			
	Average block diameter (mm)	49				21				29			
Dislocation loop	Irrad/As NT	As NT		Irradiated		As NT		Irradiated		As NT		Irradiated	
	Number density ($\times 10^{23}$/m^5)	N.A.		1.90		N.A.		1.81		N.A.		1.63	
	Average diameter (nm)	N.A.		3.43		N.A.		4.19		N.A.		3.63	
Precipitate	Amount of residue (wt%)	2.55		3.05		3.27		3.56		2.35		2.62	
	Location	Lath in matrix	Block packet, PAG	Lath in matrix	Block Packet, PAG	Lath in matrix	Block packet, PAG	Lath in matrix	Block packet, PAG	Lath in matrix	Block packet, PAG	Lath in matrix	Block Packet, PAG
	Nominal number density N/N_{total}	0.46	0.54	0.13	0.87	0.51	0.49	0.35	0.65	0.43	0.57	0.43	0.57
	Estimated number density ($\times 10^{15}$/m^3)	1.28	1.47	0.42	2.88	1.81	1.72	1.36	2.48	1.36	1.82	1.21	1.61
	Average diameter ($\sqrt{}$(Projected area)) (nm)	56.7	87.6	38.6	65.4	93.5	114.8	56.2	64.6	35.3	132.5	61.9	74.3

Estimated number density of precipitates was calculated based on the amount of residue of each RAFM and the number density obtained from NT F82H [6].

Table 2
Measured yield stress and ultimate tensile stress and calculated stress values of NT and irradiated RAFMs.

	F82H		ORNL9Cr		JLF-1	
	As NT	Irradiated	As NT	Irradiated	As NT	Irradiated
Yield stress, σ_y, (MPa)	528	838	577	1040	525	833
Ultimate tensile stress, σ_u (MPa)	600	911	734	1040	658	858
α''	0.27	–	0.44	–	0.55	–
$\Delta\tau_i$(loop) (MPa)	–	1GG	–	177	–	15G
τ_b^{irrad} (D = 300 nm) (MPa)	–	50	–	84	–	100
Estimated $\Delta\tau_y$ (MPa)	–	216	–	261	–	256
Actual $\Delta\tau_y = \Delta\sigma_y/\sqrt{3}$ (MPa)	–	213	–	267	–	181

loop or $a\langle 100\rangle$ loop, is ignored in this calculation since the average loop size is small. The calculated values clearly show that contribution of dislocation loops is not enough to explain the observed hardening level; this same tendency was pointed out by Schaublin et al. [2,3].

The irradiation-induced precipitate changes were found, but the current changes are mainly those of $M_{23}C_6$, and the number density is on the order of 10^{15}, so these precipitates are apparently not enough to explain the extra hardening level. XRD analyses on the residue obtained from the irradiated RAFMs indicated the possible nucleation of new nano-size precipitates [6,7], and this could be interpreted as the indication of the formation of Cr-rich precipitates by irradiation as observed by Wakai on heavily irradiated F82H [15], but their presence at lower doses in irradiated F82H has not been adequately verified.

The other aspect of irradiation hardening that has not been discussed is the interpretation of dislocation channel formation. It was clearly shown that dislocation loops were swept away when dislocations moved through the deformation band (Fig. 7) [16]. This indicated that the main obstacles against dislocation movement disappeared in the major deformation band. It was also indicated by true stress–true strain analyses on irradiated F82H [17] that no significant work hardening was observed, and yield stress, ultimate tensile stress and flow stress were nearly equal in irradiated F82H, although residual ductility was observed. These results suggest the possible interpretation for the yield process of irradiation-hardened RAFMs as follows:

(1) A dislocation source in a grain is activated at $\tau_{applied} = \tau_i + \Delta\tau_i$(loop).
(2) A dislocation band is formed that forms a dislocation channel and sweeps away dislocation loops; $\tau_{applied} = \tau_i + \Delta\tau_i$(loop).
(3) Dislocations pile up at the cross section of a dislocation channel and boundary, which cancel the dislocation source activation; $\tau_{applied}$ is still equal to $\tau_i + \Delta\tau_i$(loop).
(4) Yield occurs when extra dislocations pile up enough to activate a dislocation source in the adjacent grain. Here $\tau_c = \tau_i + \Delta\tau_i$(loop), and $\tau_{applied} = \tau_i + \Delta\tau_i(\text{loop}) + \tau_b^{irrad}$.

Thus, the irradiation hardening could be expressed as follows:

$$\Delta\tau_y = \Delta\tau_i(\text{loop}) + \tau_b^{irrad} = \alpha_{loop} Gb\sqrt{N_{loop}\cdot d_{loop}} + \frac{k_y^{applied}}{\sqrt{D}}, \quad (8)$$

$$k_y^{irrad} = \alpha''\sqrt{Gb(\tau_i + \Delta_i(\text{loop}))}. \quad (9)$$

If we roughly assume that α'', D and τ_i are same as that of unirradiated RAFM and $\tau_i + \Delta\tau_y = \frac{1}{\sqrt{3}}\sigma_y^{irrad}$, then the calculation suggests that there is good agreement for F82H and ORNL 9Cr, but not for JLF-1 (Table 2). This result suggests the possibility that the extra hardening addition to the dislocation loop hardening could be the effect of back stress becoming significant during the yield process for irradiated RAFMs, and the discrepancy in the case of JLF-1 might be because precipitate recovery is enhanced in irradiated JLF-1 [6,7], and that causes the changes of the blocking distance D or α'' and decreases the effect of back stress. A detailed microstructure analyses on irradiated RAFMs deformed to various levels is required to examine the validity of this mechanism, and such tests will be conducted in near future.

4. Summary

Various microstructural analyses on RAFMs irradiated at 300 °C up to 5 dpa were summarized with the emphasis on F82H, and a possible irradiation-hardening mechanism was suggested as follows.

- Dislocation-loop hardening described by the Orowan equation is not enough to explain various irradiation-hardening observations in RAFMs.
- The back-stress effect described by the Hall–Petch equation, which is supposed to be observed in the strain-hardening process in normalized-and-tempered RAFMs, could be the extra contributor to irradiation hardening, as plastic deformation is limited in a dislocation channel and extra applied stress equivalent to a back stress could be required to activate dislocation sources in an adjacent grain.
- Irradiation hardening could be the sum of the friction stress increase caused by dislocation loop formation and the back stress, which becomes significant as the deformation is limited in dislocation channeling.
- Irradiation induced precipitation changes might change the back-stress effects.

References

[1] K.E. Lenox, M.L. Grossbeck, DOE/ER-313/25, 1998, p. 307.
[2] R. Schaublin, P. Spatig, M. Victoria, J. Nucl. Mater. 258–263 (1998) 1178.
[3] R. Schaublin, D. Gelles, M. Victoria, J. Nucl. Mater. 307–311 (2002) 197.
[4] D.S. Gelles, J. Nucl. Mater. 329–333 (2004) 304.
[5] H. Tanigawa, M. Ando, Y. Katoh, T. Hirose, H. Sakasegawa, S. Jitsukawa, A. Kohyama, T. Iwai, J. Nucl. Mater. 297 (2001) 279.
[6] H. Tanigawa, H. Sakasegawa, N. Hashimoto, R.L. Klueh, M. Ando, M.A. Sokolov, J. Nucl. Mater. 367–370 (2007) 42.
[7] H. Tanigawa, H. Sakasegawa, R.L. Klueh, Mater. Trans. JIM 46 (2005) 469.
[8] H. Tanigawa, H. Sakasegawa, H. Ogiwara, H. Kishimoto, A. Kohyama, J. Nucl. Mater. 367–370 (2007) 132.
[9] E. Wakai, Y. Miwa, N. Hashimoto, J.P. Robertson, R.L. Klueh, K. Shiba, K. Abiko, S. Furuno, S. Jitsukawa, J. Nucl. Mater. 307–311 (2002) 203.
[10] X. Jia, Y. Dai, M. Victoria, J. Nucl. Mater. 305 (2002) 1.
[11] L.A. Norstorm, Scand. J. Metall. 5 (1976) 159.
[12] R.W. Hertzberg, Deformation and Fracture Mechanics of Engineeering Materials, John Wiley, 1996.
[13] E. Hornbogen, G. Staniek, J. Mater. Sci. 9 (1974) 879.
[14] E. Wakai, A. Hishinuma, K. Usami, Y. Kato, S. Takaki, K. Abiko, Mater. Trans. JIM 41 (2000) 1180.
[15] E. Wakai, Y. Miwa, N. Hashimoto, J.P. Robertoson, R.L. Klueh, K. Shiba, K. Abiko, S. Furuno, S. Jistukawa, J. Nucl. Mater. 307–311 (2002) 20.
[16] N. Hashimoto, M. Ando, H. Tanigawa, T. Sawai, K. Shiba, R.L. Klueh, Fus. Sci. Technol. 44 (2003) 490.
[17] T. Taguchi, S. Jitsukawa, M. Sato, S. Matsukawa, E. Wakai, K. Shiba, J. Nucl. Mater. 335 (2004) 457.